AIAA SciTech Forum
23-27 January 2023, National Harbor, MD & Online
AIAA SCITECH 2023 Forum

10.2514/6.2023-1984

Structured Input-Output Analysis of Compressible Plane Couette Flow

Diganta Bhattacharjee*
University of Minnesota, Minneapolis, MN 55455, USA

Talha Mushtaq†
University of Minnesota, Minneapolis, MN 55455, USA

Peter Seiler‡
University of Michigan, Ann Arbor, MI 48109, USA

Maziar S. Hemati§
University of Minnesota, Minneapolis, MN 55455, USA

This paper extends the recently introduced structured input-output analysis method for incompressible flows to the compressible regime. The proposed method relies upon an exact quadratic representation of the compressible Navier-Stokes equations that allows for efficient modeling and analysis within the structured singular value framework. Specifically, the compressible plane Couette flow is investigated and the structure of the nonlinear forcing is used to formulate an input-output model suitable for the structured singular value analysis. We have outlined an efficient method to compute upper bounds on the structured singular value, which provide insight into flow instability. Numerical results of the proposed framework are included for subsonic, transonic, and supersonic Mach numbers. These results are compared with those obtained from resolvent gain and unstructured input-output analysis. Our findings show that accounting for the structure of the nonlinearity not only reduces the conservatism in the unstructured gains—thereby increasing the estimated stability margin—but also eliminates some of the instability mechanisms predicted by these other analysis tools. Moreover, the structured input-output results reveal instability mechanisms that are not captured by the resolvent analysis. These contradictory findings between the analysis techniques considered need to be substantiated through experimental and/or computational studies in the future.

I. Introduction

Compressible flows arise in most aerospace applications. These flows are governed by the compressible Navier-Stokes equations (NSE), which can result in highly complex flow physics with a rich array of nonlinear flow interactions. Modal analysis techniques have proven to be invaluable for unraveling these complex flow physics to arrive at an improved understanding of key instability mechanisms and coherent structures that drive the associated fluid dynamics [1–3]. Input-output (I/O) and resolvent-based techniques have established themselves as key tools in the arsenal [4]. These techniques were primarily adopted and developed in the context of incompressible flows [5, 6], but have since been adopted and developed for studies of compressible fluid dynamics [7–11]. I/O methods are inherently physics-based and work by decomposing the governing equations into a feedback interconnection between the linear dynamics and the nonlinear terms. Traditionally, the outputs of the nonlinear terms are treated as an implicit (unstructured) forcing on the linear dynamics, which results in an optimization problem that is relatively straightforward to solve using linear systems analysis techniques. Despite their successes, linear I/O analysis neglects any known structure regarding the nonlinear terms. Most existing analysis methods that account for these nonlinearities result in computationally expensive—or even intractable—solution algorithms [12–16].

*Postdoctoral Research Associate, Aerospace Engineering and Mechanics, AIAA Member.
†Graduate Research Assistant, Aerospace Engineering and Mechanics.
‡Associate Professor, Electrical Engineering and Computer Science, and AIAA Associate Fellow.
§Associate Professor, Aerospace Engineering and Mechanics, AIAA Associate Fellow

Recently, a structured I/O analysis framework was proposed within the context of incompressible flows that provides a computationally tractable method for imposing structural information about the nonlinear terms within the linear I/O analysis framework [17]. This approach extends established ideas from the robust controls literature [18, 19] to the context of incompressible fluid dynamics for which the (convective) nonlinear terms are quadratic. It was further shown in [20] that additional repeated structure in the convective nonlinearity in the incompressible NSE can be exploited to further refine the structured I/O analysis. Moreover, the structured I/O framework can be utilized to conduct modal analysis, as shown in [21].

In this paper, we investigate the utility of structured I/O methods for the analysis of compressible flows. The nonlinear terms in the compressible NSE are substantially more complicated than in the incompressible NSE. In most systems-theoretic formulations, the nonlinearity in the compressible NSE is cubic [22], which creates non-trivial challenges with regards to the necessary uncertainty modeling of the nonlinear terms for subsequent structured I/O analysis. Here, we will exploit a reformulation of the compressible NSE for which the resulting nonlinearity is quadratic. The nonlinearity in this reformulation is still substantially more complicated than for incompressible flows, but makes the application of structured I/O analysis more tractable. For this investigation, we consider a compressible plane Couette flow over a range of Mach numbers. This flow has been investigated in numerous other works on stability and I/O analysis due to its simplicity [8, 23, 24]. Results of the structured I/O analysis are compared with those obtained from resolvent gain and unstructured input-output (using the H_∞ norm) analysis. Included numerical results illustrate that accounting for the structure of the nonlinearity not only reduces the conservatism in the unstructured gains (which translates to a larger margin of stability) but also eliminates some of the possibly redundant instability mechanisms predicted by these other analysis tools. Moreover, the structured I/O results reveal different instability mechanisms that are not predicted in the resolvent gain results.

The remainder of the paper proceeds as follows. The exact quadratic representation of compressible NSE and relevant details are provided in Section II. The compressible plane Couette flow problem is elaborated in Section III which includes details on the base flow calculations, perturbation dynamics, and structured I/O analysis. Section IV contains the simulation results and the conclusions of this work are provided in Section V.

We use symbols $\mathbb{C}^n$, $\mathbb{C}^{n\times m}$ and $\mathbb{R}^{n\times m}$ to denote the sets of n-dimensional complex vectors, complex matrices of dimension $n \times m$, real matrices of dimension $n \times m$, respectively. The symbols $\|\cdot\|_2$ and $\|\cdot\|_F$ respectively denote the spectral and Frobenius norms of a matrix. Also, an $n \times n$ identity matrix is denoted by $\mathbf{I}_n$ and we use $\mathbf{i} = \sqrt{-1}$ as the imaginary unit.

II. Quadratic Representation of Compressible Navier-Stokes Equations

Consider a compressible fluid in the domain $\Omega \subset \mathbb{R}^3$. The state of the fluid at any instant in time can be characterized solely based on the primitive variables of density $\varrho(\mathbf{x}, t)$, velocity $\mathbf{u}(\mathbf{x}, t) = (u(\mathbf{x}, t), v(\mathbf{x}, t), w(\mathbf{x}, t))$, and pressure $p(\mathbf{x}, t)$. Here, $\mathbf{x} \in \Omega$ is the spatial coordinate and $t \in \mathbb{R}$ is time. The equations of motion governing the dynamics of the flow in Ω are derived from the conservation laws for mass, momentum, and energy. These equations can be expressed in terms of the primitive variables $\mathbf{q} = (\xi := 1/\varrho, \mathbf{u}, p)$. All variables are non-dimensionalized in the usual way using L, u_r, T_r, $\xi_r = 1/\rho_r$, and η_r as the reference length, velocity, temperature, specific volume (density), and viscosity, respectively. The reference pressure is chosen to be $p_r = T_r R/\xi_r$. Denoting all dimensional quantities with a superscript $(\cdot)^d$, we define the following non-dimensional quantities:

$$\xi = \frac{\xi^d}{\xi_r}, \quad \mathbf{u} = \frac{\mathbf{u}^d}{u_r}, \quad t = \frac{t^d}{L/u_r}, \quad \eta = \frac{\eta^d}{\eta_r}, \quad T = \frac{T^d}{T_r}, \quad p = \frac{p^d}{p_r}, \quad Re = \frac{u_r L}{\eta_r \xi_r}, \quad M_r = \frac{u_r}{a_r} = \frac{u_r}{\sqrt{\gamma R T_r}}, \tag{1}$$

where η is the coefficient of shear viscosity, while Re and M_r denote the Reynolds number and Mach number, respectively. The resulting non-dimensional compressible Navier-Stokes equations can be expressed as

$$\partial_t \xi + \mathbf{u} \cdot \nabla \xi - \xi \nabla \cdot \mathbf{u} = 0 \tag{2}$$

$$\partial_t \mathbf{u} + \mathbf{u} \cdot \nabla \mathbf{u} = -\frac{1}{\gamma M_r^2} \xi \nabla p + \frac{1}{Re} \xi \nabla \cdot \Pi(\mathbf{u}, \eta) \tag{3}$$

$$\partial_t p + \mathbf{u} \cdot \nabla p + \gamma p \nabla \cdot \mathbf{u} = \frac{\gamma(\gamma - 1) M_r^2}{Re} \Phi(\mathbf{u}, \eta) + \frac{\gamma}{RePr} \nabla \cdot (\eta \nabla (p\xi)) \tag{4}$$

with the associated non-dimensional equation of state for a perfect polytropic gas $p\xi = T$. Here, $\Pi(\mathbf{u}, \eta)$ denotes the viscous stress tensor, which for a Newtonian fluid takes the form

$$\Pi(\mathbf{u}, \eta) = \begin{bmatrix} \tau_{xx} & \tau_{xy} & \tau_{xz} \\ \tau_{yx} & \tau_{yy} & \tau_{yz} \\ \tau_{zx} & \tau_{zy} & \tau_{zz} \end{bmatrix} = 2\eta D + (\eta_b - \frac{2}{3}\eta)(\nabla \cdot \mathbf{u})I,$$

where η_b is the coefficient of bulk viscosity, and D is the deformation tensor given by

$$D = \begin{bmatrix} \partial_x u & \frac{1}{2}(\partial_x v + \partial_y u) & \frac{1}{2}(\partial_x w + \partial_z u) \\ \frac{1}{2}(\partial_y u + \partial_x v) & \partial_y v & \frac{1}{2}(\partial_y w + \partial_z v) \\ \frac{1}{2}(\partial_z u + \partial_x w) & \frac{1}{2}(\partial_z v + \partial_y w) & \partial_z w \end{bmatrix}.$$

In this work, we will apply Stokes' hypothesis, so that $\eta_b = 0$. Also, the term $\Phi(\mathbf{u}, \eta)$ in (4) is the viscous dissipation term given by

$$\begin{aligned} \Phi(\mathbf{u}, \eta) &= \eta \left(2 \left((\partial_x u)^2 + (\partial_y v)^2 + (\partial_z w)^2 \right) + (\partial_y u + \partial_x v)^2 + (\partial_z v + \partial_y w)^2 + (\partial_z u + \partial_x w)^2 \right) - \frac{2}{3}\eta(\nabla \cdot \mathbf{u})^2 \\ &= \frac{\eta}{2} \left[\nabla \mathbf{u} + (\nabla \mathbf{u})^{\mathrm{T}} \right]^2 - \frac{2}{3}\eta(\nabla \cdot \mathbf{u})^2. \end{aligned} \tag{5}$$

Next, we consider the dynamics of perturbations about a steady base flow $(\xi_0, \mathbf{u}_0, p_0, T_0, \eta_0)$ with $\mathbf{u}_0 = (u_0, v_0, w_0)$. We will assume temperature dependence of the viscosity in the base flow calculation $\eta_0 = \eta_0(T_0)$; however, the temperature dependence of viscosity in the perturbation dynamics—and therefore perturbations to the base viscosity η_0—will be neglected in the ensuing analysis. Isolating the linear dynamics on the left-hand side and the nonlinear terms on the right-hand side, the dynamics of perturbations can be expressed as

$$\partial_t \xi - L_\xi(\mathbf{q}) = Q_\xi(\mathbf{q}) \tag{6}$$

$$\partial_t \mathbf{u} - L_\mathbf{u}(\mathbf{q}) = Q_\mathbf{u}(\mathbf{q}) \tag{7}$$

$$\partial_t p - L_p(\mathbf{q}) = Q_p(\mathbf{q}) \tag{8}$$

$$T - L_T(\mathbf{q}) = Q_T(\mathbf{q}) \tag{9}$$

where $\mathbf{q} = (\xi, \mathbf{u}, p)$ is the vector of perturbed quantities, and

$$\begin{aligned} L_\xi(\mathbf{q}) &= -\mathbf{u}_0 \cdot \nabla \xi - \mathbf{u} \cdot \nabla \xi_0 + \xi \nabla \cdot \mathbf{u}_0 + \xi_0 \nabla \cdot \mathbf{u} \\ L_\mathbf{u}(\mathbf{q}) &= -\mathbf{u}_0 \cdot \nabla \mathbf{u} - \mathbf{u} \cdot \nabla \mathbf{u}_0 - \xi_0 \nabla p - \xi \nabla p_0 + \frac{1}{Re} \left(\xi \nabla \cdot \Pi(\mathbf{u}_0, \eta_0) + \xi_0 \nabla \cdot \Pi(\mathbf{u}, \eta_0) \right) \\ L_p(\mathbf{q}) &= -\mathbf{u}_0 \cdot \nabla p - \mathbf{u} \cdot \nabla p_0 - \gamma \left(p \nabla \cdot \mathbf{u}_0 + p_0 \nabla \cdot \mathbf{u} \right) + \frac{\gamma(\gamma-1)M_r^2}{Re} \Bigg(\eta_0 \Big(4\partial_x u \partial_x u_0 + 4\partial_y v \partial_y v_0 + 4\partial_z w \partial_z w_0 \\ &\quad + 2(\partial_y u + \partial_x v)(\partial_y u_0 + \partial_x v_0) + 2(\partial_z v + \partial_y w)(\partial_z v_0 + \partial_y w_0) + 2(\partial_z u + \partial_x w)(\partial_z u_0 + \partial_x w_0) \Big) \\ &\quad - \frac{4}{3}\eta_0(\nabla \cdot \mathbf{u}_0)(\nabla \cdot \mathbf{u}) \Bigg) + \frac{\gamma}{RePr} \nabla \cdot \eta_0 \left(\nabla(p_0 \xi + p \xi_0) \right) \\ L_T(\mathbf{q}) &= p_0 \xi + p \xi_0 \\ Q_\xi(\mathbf{q}) &= \xi \nabla \cdot \mathbf{u} - \mathbf{u} \cdot \nabla \xi \\ Q_\mathbf{u}(\mathbf{q}) &= -\mathbf{u} \cdot \nabla \mathbf{u} - \xi \nabla p + \frac{1}{Re} \xi \nabla \cdot \Pi(\mathbf{u}) \\ Q_p(\mathbf{q}) &= -\mathbf{u} \cdot \nabla p - \gamma p \nabla \mathbf{u} + \frac{\gamma(\gamma-1)M_r^2}{Re} \Phi(\mathbf{u}, \eta_0) + \frac{\gamma}{RePr} \nabla \cdot (\eta_0 \nabla(p\xi)) \\ Q_T(\mathbf{q}) &= p\xi. \end{aligned}$$

The partitioning into linear and nonlinear terms facilitates the formulation of the structured I/O problem. We will demonstrate this in the context of a compressible plane Couette flow in the next section.

III. Structured I/O Analysis of Compressible Plane Couette Flow

The compressible plane Couette flow is a convenient canonical setup for investigation that has been considered in many prior works—see, e.g., [8, 23–25].

A. Steady Base Flow

The base profile can be computed with relative ease: it can be shown that the base temperature profile $T_0(y)$ will be a second-order polynomial function of the streamwise base velocity profile $U_0(y)$ [23]. Further, this base flow profile will be independent of the Reynolds number Re. Here we will show that the same conclusion can be drawn from the non-dimensional quadratic representation of the compressible NSE. Assume a base profile with $(u, v, w) = (U_0(y), 0, 0)$, $\xi = \xi_0(y)$, and $p = p_0(y)$. The continuity and z-momentum equations will be satisfied automatically. It follows from the y-momentum equation that the base pressure profile will actually be a constant, which we will take to be unity: $p_0(y) = p_0 = 1$. The x-momentum equation shows that the base shear-stress profile $\tau_0 = \eta_0 \, (\partial U_0/\partial y)$ will be constant:

$$\frac{\mathrm{d}}{\mathrm{d}y}\left(\eta_0 \frac{\mathrm{d}U_0}{\mathrm{d}y}\right) = 0. \tag{10}$$

The energy equation reduces to the condition:

$$\frac{\mathrm{d}}{\mathrm{d}y}\left((\gamma-1)M_r^2\tau_0 U_0 + \frac{\eta_0}{Pr}\frac{\mathrm{d}T_0}{\mathrm{d}y}\right) = 0, \tag{11}$$

where we have utilized the equation of state $\xi_0(y) = T_0(y)$ since $p_0 = 1$. The boundary conditions are taken to be

$$U_0(0) = 0, \quad U_0(1) = 1, \quad T_0(0) = T_L, \quad T(1) = 1, \tag{12}$$

where T_L is the mean temperature of the lower wall. Now, we can integrate (11) to obtain the baseflow temperature profile as [23, 24]

$$T_0 = T_{rec}\left[r + (1-r)U_0 - (1 - T_{rec}^{-1})U_0^2\right], \tag{13}$$

where we have defined the recovery temperature $T_{rec} = 1 + (\gamma-1)PrM_r^2/2$ and recovery factor $r = T_L/T_{rec}$. For consistency with this prior work, we assume temperature dependence of the base viscosity according to Sutherland's law:

$$\eta_0 = \frac{T_0^{3/2}(1+C)}{T_0 + C}, \quad \text{with } C = 0.5. \tag{14}$$

The base velocity profile can be computed from (10). Since the shear stress τ_0 is an unknown constant, this can be done iteratively together with (13) and (14). Here, we use a shooting method composed of a fourth order Runge-Kutta integration scheme in conjunction with a secant method for determining the initial condition for the next iterate. The process is then repeated until convergence. Base profiles for $Pr = 0.72$, $r = 1$ (adiabatic lower wall), and $M_r = (0.5, 1, 2)$ are shown in Fig. 1. As noted in [23], beginning with a monotone initial guess for $U_0(y)$ facilitates convergence. For the cases considered in our study, convergence of the shooting method to an absolute error of $\epsilon \leq 10^{-8}$ between iterates required $\sim O(10)$ total iterations.

B. Perturbation Dynamics about the Steady Base Flow

The perturbation dynamics about the steady base flow is given by

$$\begin{aligned}
&\partial_t \xi + U_0\partial_x\xi + v\xi_0' - \xi_0\nabla\cdot\mathbf{u} = -\mathbf{u}\cdot\nabla\xi + \xi\nabla\cdot\mathbf{u}\\
&\partial_t \mathbf{u} + U_0\partial_x\mathbf{u} + vU_0'\mathbf{e}_x + \frac{1}{\gamma M_r^2}\xi_0\nabla p - \frac{\xi_0}{Re}\nabla\cdot\Pi(\mathbf{u},\eta_0) = -\frac{1}{\gamma M_r^2}\xi\nabla p - \mathbf{u}\cdot\nabla\mathbf{u} + \frac{\xi}{Re}\nabla\cdot\Pi(\mathbf{u},\eta_0)\\
&\partial_t p + U_0\partial_x p + \gamma p_0\nabla\cdot\mathbf{u} - \frac{\gamma(\gamma-1)M_r^2}{Re}\left(2\eta_0 U_0'(\partial_y u + \partial_x v)\right)\\
&- \frac{\gamma}{RePr}\left(\eta_0 p_0\nabla^2\xi + \eta_0\xi_0\nabla^2 p + 2\eta_0\xi_0'\partial_y p + \eta_0\xi_0'' p + \eta_0'\left(p_0\partial_y\xi + p\xi_0' + \xi_0\partial_y p\right)\right)\\
&= -\mathbf{u}\cdot\nabla p - \gamma p\nabla\cdot\mathbf{u} + \frac{\gamma(\gamma-1)M_r^2}{Re}\Phi(\mathbf{u},\eta_0) + \frac{\gamma}{RePr}\left(\eta_0\nabla^2(p\xi) + \xi\nabla p\cdot\nabla\eta_0 + p\nabla\xi\cdot\nabla\eta_0\right)
\end{aligned} \tag{15}$$

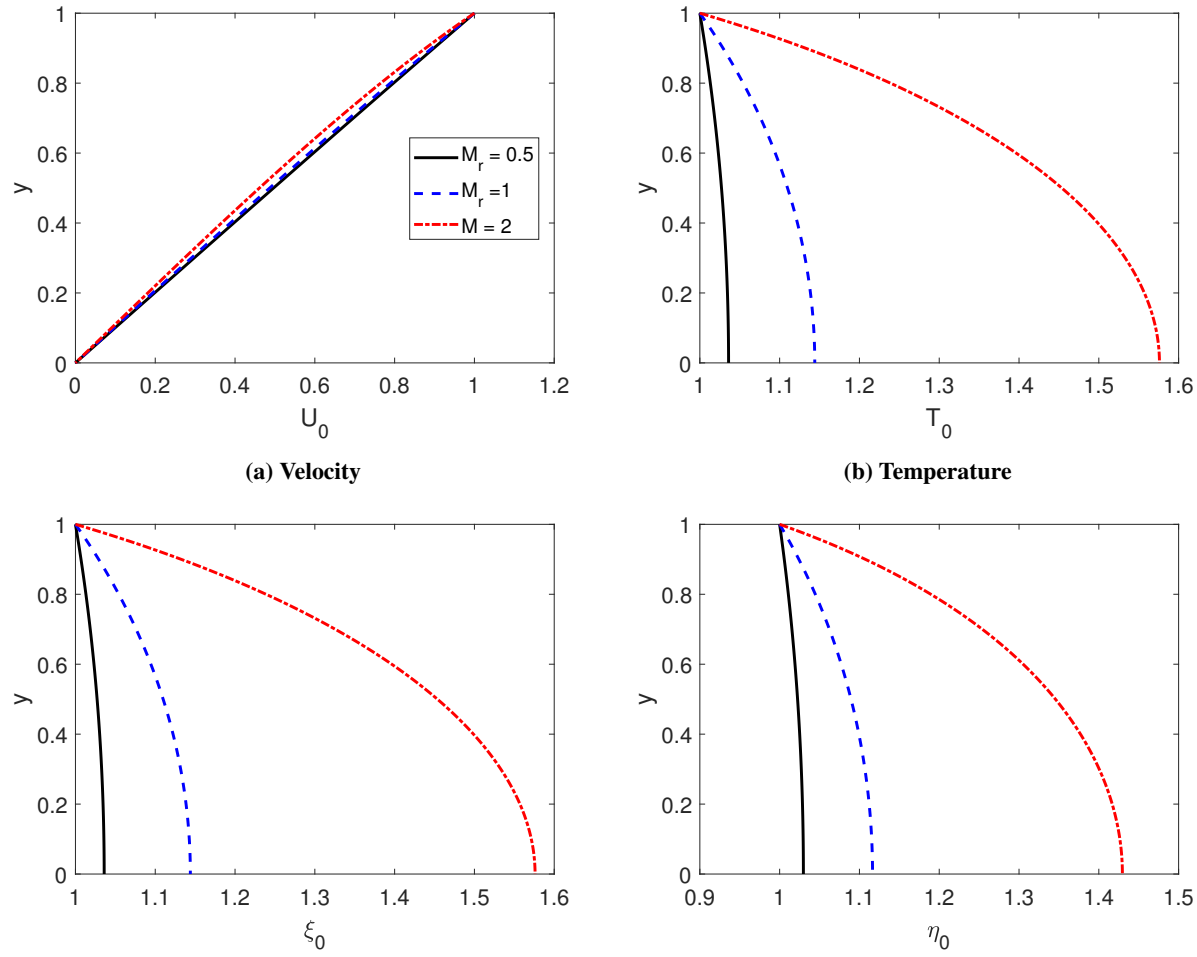

(a) Velocity **(b) Temperature**

(c) Specific volume **(d) Viscosity coefficient**

Fig. 1 Steady base flow profiles for compressible plane Couette flow for different Mach numbers.

where $\mathbf{e}_x$ is the unit vector for the x direction, $(\cdot)' = \mathrm{d}(\cdot)/\mathrm{d}y$ and $(\cdot)'' = \mathrm{d}^2(\cdot)/\mathrm{d}y^2$ for the associated base flow quantities. Therefore, the linear operators for the perturbation dynamics about the steady base flow reduce to

$$
\begin{aligned}
L_\xi(\mathbf{q}) &= -U_0\partial_x\xi - v\xi_0' + \xi_0\nabla\cdot\mathbf{u} \\
L_u(\mathbf{q}) &= -U_0\partial_x u - U_0'v - \frac{1}{\gamma M_r^2}\xi_0\partial_x p + \frac{\xi_0}{Re}\left[\eta_0\left(\nabla^2 u + \frac{1}{3}(\partial_{xx}u + \partial_{xy}v + \partial_{xz}w)\right) + (\partial_y u + \partial_x v)\eta_0'\right] \\
L_v(\mathbf{q}) &= -U_0\partial_x v - \frac{1}{\gamma M_r^2}\xi_0\partial_y p + \frac{\xi_0}{Re}\left[\eta_0\left(\nabla^2 v + \frac{1}{3}(\partial_{xy}u + \partial_{yy}v + \partial_{yz}w)\right) + \left(\frac{4}{3}\partial_y v - \frac{2}{3}(\partial_z w + \partial_x u)\right)\eta_0'\right] \\
L_w(\mathbf{q}) &= -U_0\partial_x w - \frac{1}{\gamma M_r^2}\xi_0\partial_z p + \frac{\xi_0}{Re}\left[\eta_0\left(\nabla^2 w + \frac{1}{3}(\partial_{xz}u + \partial_{yz}v + \partial_{zz}w)\right) + (\partial_z v + \partial_y w)\eta_0'\right] \\
L_p(\mathbf{q}) &= -U_0\partial_x p - \gamma p_0\nabla\cdot\mathbf{u} + \frac{\gamma(\gamma-1)M_r^2}{Re}\left(2\eta_0 U_0'(\partial_y u + \partial_x v)\right) \\
&\quad + \frac{\gamma}{RePr}\left(\eta_0 p_0\nabla^2\xi + \eta_0\xi_0\nabla^2 p + 2\eta_0\xi_0'\partial_y p + \eta_0\xi_0'' p + \eta_0'\left(p_0\partial_y\xi + p\xi_0' + \xi_0\partial_y p\right)\right).
\end{aligned}
\tag{16}
$$

No-slip and impermeability boundary conditions are applied to velocity perturbations at both walls, i.e., $u(0) = u(1) = v(0) = v(1) = w(0) = w(1) = 0$. In this work, we assume an adiabatic lower wall (i.e., $\partial_y T(0) = 0$) and an isothermal

upper wall (i.e., $T(1) = 0$). These translate to the following conditions on specific volume and pressure at the boundaries:

$$\partial_y p(0)\xi_0(0) + \partial_y \xi(0) + \partial_y (p\xi)(0) = 0, \tag{17}$$

$$p(1)\xi_0(1) + \xi(1)(1 + p(1)) = 0. \tag{18}$$

These conditions are satisfied by imposing homogeneous Dirichlet and Neumann boundary conditions, i.e., $\xi(1) = p(1) = 0$ and $\partial_y \xi(0) = \partial_y p(0) = 0$.

With the linear operators as defined above, the perturbation dynamics (15) can now be expressed as

$$\partial_t \xi = L_\xi(\mathbf{q}) + f_\xi(\mathbf{q}), \quad \partial_t \mathbf{u} = L_\mathbf{u}(\mathbf{q}) + f_\mathbf{u}(\mathbf{q}), \quad \partial_t p = L_p(\mathbf{q}) + f_p(\mathbf{q}), \tag{19}$$

where $L_\mathbf{u}(\mathbf{q}) = \begin{bmatrix} L_u(\mathbf{q}) & L_v(\mathbf{q}) & L_w(\mathbf{q}) \end{bmatrix}^\mathrm{T}$ and the nonlinear forcings are

$$\begin{aligned} f_\xi(\mathbf{q}) &= -\mathbf{u}\cdot\nabla\xi + \xi\nabla\cdot\mathbf{u}, \quad f_\mathbf{u}(\mathbf{q}) = -\frac{1}{\gamma M_r^2}\xi\nabla p - \mathbf{u}\cdot\nabla\mathbf{u} + \frac{\xi}{Re}\nabla\cdot\Pi(\mathbf{u},\eta_0), \\ f_p(\mathbf{q}) &= -\mathbf{u}\cdot\nabla p - \gamma p\nabla\cdot\mathbf{u} + \frac{\gamma(\gamma-1)M_r^2}{Re}\Phi(\mathbf{u},\eta_0) + \frac{\gamma}{RePr}\left(\eta_0\nabla^2(p\xi) + \xi\nabla p\cdot\nabla\eta_0 + p\nabla\xi\cdot\nabla\eta_0\right). \end{aligned} \tag{20}$$

This description of the perturbation dynamics in (19) provides a systems-theoretic (or feedback) interpretation of the equations, which is shown in Fig. 2a where the perturbed quantities $(\xi, \mathbf{u}, p)$ denote the state of a linear system (i.e., the linear perturbation dynamics). The states are also the outputs of the linear system and the inputs forcing the linear system are nonlinear feedback of the outputs (see Fig. 2a). Furthermore, the term $\Phi(\mathbf{u},\eta_0)$ can be expressed as

$$\Phi(\mathbf{u},\eta_0) = \frac{\eta_0}{2}\left[\nabla\mathbf{u} + (\nabla\mathbf{u})^\mathrm{T}\right]^2 - \frac{2}{3}\eta_0(\nabla\cdot\mathbf{u})^2 = \frac{\eta_0}{2}\Psi_1(\mathbf{u}) - \frac{2}{3}\eta_0\Psi_2(\mathbf{u}) \tag{21}$$

where

$$\Psi_1(\mathbf{u}) = \begin{bmatrix} (\nabla u)^\mathrm{T} & (\nabla v)^\mathrm{T} & (\nabla w)^\mathrm{T} & (\partial_x\mathbf{u})^\mathrm{T} & (\partial_y\mathbf{u})^\mathrm{T} & (\partial_z\mathbf{u})^\mathrm{T} \end{bmatrix} \begin{bmatrix} \nabla u \\ \nabla v \\ \nabla w \\ (2\nabla u + \partial_x\mathbf{u}) \\ (2\nabla v + \partial_y\mathbf{u}) \\ (2\nabla w + \partial_z\mathbf{u}) \end{bmatrix}, \ \Psi_2(\mathbf{u}) = (\nabla\cdot\mathbf{u})^2. \tag{22}$$

Also, we have the following identity

$$\nabla^2(p\xi) = \xi\nabla^2 p + p\nabla^2\xi + 2\nabla p\cdot\nabla\xi. \tag{23}$$

After substituting the above expressions in (20), we derive

$$\begin{aligned} f_\xi(\mathbf{q}) &= -\mathbf{u}\cdot\nabla\xi + \xi\nabla\cdot\mathbf{u}, \qquad f_\mathbf{u}(\mathbf{q}) = -\frac{1}{\gamma M_r^2}\xi\nabla p - \mathbf{u}\cdot\nabla\mathbf{u} + \frac{\xi}{Re}\nabla\cdot\Pi(\mathbf{u},\eta_0), \\ f_p(\mathbf{q}) &= -\mathbf{u}\cdot\nabla p - \gamma p\nabla\cdot\mathbf{u} + \frac{\gamma(\gamma-1)M_r^2}{Re}\frac{\eta_0}{2}\Big[(\nabla u)^\mathrm{T}\nabla u + (\nabla v)^\mathrm{T}\nabla v + (\nabla w)^\mathrm{T}\nabla w \\ &\quad + (\partial_x\mathbf{u})^\mathrm{T}(2\nabla u + \partial_x\mathbf{u}) + (\partial_y\mathbf{u})^\mathrm{T}(2\nabla v + \partial_y\mathbf{u}) + (\partial_z\mathbf{u})^\mathrm{T}(2\nabla w + \partial_z\mathbf{u})\Big] - \frac{\gamma(\gamma-1)M_r^2}{Re}\frac{2}{3}\eta_0(\nabla\cdot\mathbf{u})^2 \\ &\quad + \frac{\gamma}{RePr}\left(\eta_0\xi\nabla^2 p + \eta_0 p\nabla^2\xi + 2\eta_0\nabla p\cdot\nabla\xi + \nabla\eta_0\cdot\xi\nabla p + \nabla\eta_0\cdot p\nabla\xi\right). \end{aligned} \tag{24}$$

C. Modeling the Nonlinear Terms: Structured Uncertainty

We now describe a modeling of the quadratic nonlinearities in (24), collectively denoted by a vector $\mathbf{f}$, that enables the structured I/O analysis using the structured singular value formalism. This involves separating each quadratic nonlinearity

into its constituent linear parts and approximating one of the linear parts as an uncertain gain. Following the terminology used in the robust controls literature, we refer to the resulting gain matrix as a structured uncertainty which typically has a block-diagonal structure. In fact, the modeling actually requires a couple of linear transformations/operators to make the structured uncertainty block-diagonal—one each for the inputs and outputs of the structured uncertainty. The system modeling and resulting approximated system are schematically shown in Fig. 2b where the subscript $(\cdot)_\chi$ denotes approximated quantities. Therefore, the I/O modeling approximates the nonlinearity by a quasi-nonlinearity that neglects the dependence of the mapping on the states that make up both $\mathbf{y}$ and $\mathbf{f}$, i.e., the uncertainty is treated as independent of these signals. Despite this approximation, structured I/O framework provides a systematic approach to treat the nonlinearities compared to the traditional unstructured I/O techniques. This is evidenced by the structured I/O analysis of incompressible flows in [17], which led to results that were in agreement with both experimental observations and direct numerical simulation results. This indicates the usefulness of structured I/O analysis, even with the above mentioned inexactness of the modeling, and serves as a motivation for the I/O model in our research. The details of our model are provided next.

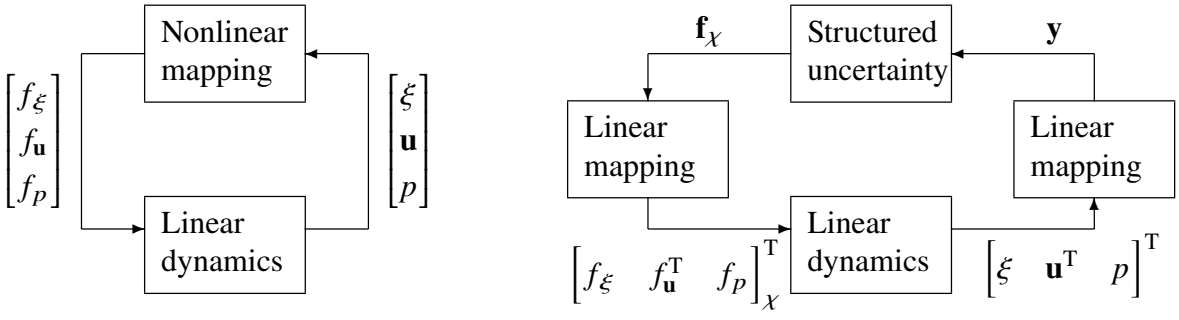

(a) Original system **(b) Approximated system**

Fig. 2 The perturbation dynamics expressed in feedback forms - both the original system and the system obtained through the modeling approximation, with subscript $(\cdot)_\chi$ denoting approximated quantities.

First, we separate out the nonlinear terms in (24) into three different vectors as

$$\mathbf{f}_1 = \begin{bmatrix} \xi\nabla^2 p \\ \xi\nabla p \\ \xi(\nabla\cdot\mathbf{u}) \\ \xi\nabla\cdot\Pi(\mathbf{u},\eta_0) \\ p\nabla^2\xi \\ p\nabla\xi \\ p\nabla\cdot\mathbf{u} \end{bmatrix}, \quad \mathbf{f}_2 = \begin{bmatrix} \mathbf{u}\cdot\nabla\xi \\ \mathbf{u}\cdot\nabla u \\ \mathbf{u}\cdot\nabla v \\ \mathbf{u}\cdot\nabla w \\ \mathbf{u}\cdot\nabla p \end{bmatrix}, \quad \mathbf{f}_3 = \begin{bmatrix} \nabla u\cdot\nabla u \\ \nabla v\cdot\nabla v \\ \nabla w\cdot\nabla w \\ \partial_x\mathbf{u}\cdot(2\nabla u+\partial_x\mathbf{u}) \\ \partial_y\mathbf{u}\cdot(2\nabla v+\partial_y\mathbf{u}) \\ \partial_z\mathbf{u}\cdot(2\nabla w+\partial_z\mathbf{u}) \\ \nabla p\cdot\nabla\xi \\ (\nabla\cdot\mathbf{u})^2 \end{bmatrix}. \tag{25}$$

These are related to the nonlinear forcings in (24) as

$$\begin{bmatrix} f_\xi \\ f_{\mathbf{u}} \\ f_p \end{bmatrix} = \mathbf{B}_1\mathbf{f}_1 + \mathbf{B}_2\mathbf{f}_2 + \mathbf{B}_3\mathbf{f}_3 = \begin{bmatrix} \mathbf{B}_1 & \mathbf{B}_2 & \mathbf{B}_3 \end{bmatrix} \begin{bmatrix} \mathbf{f}_1 \\ \mathbf{f}_2 \\ \mathbf{f}_3 \end{bmatrix} = \mathbf{B}\mathbf{f} \tag{26}$$

where $\mathbf{B}_2 = -\mathbf{I}_5$ and

$$\mathbf{B}_1 = \begin{bmatrix} 0 & 0 & 1 & 0 & 0 & 0 & 0 \\ 0 & -\frac{1}{\gamma M_r^2}\mathbf{I}_3 & 0 & \frac{1}{Re}\mathbf{I}_3 & 0 & 0 & 0 \\ c_3\eta_0 & c_3(\nabla\eta_0)^{\mathrm{T}} & 0 & 0 & c_3\eta_0 & c_3(\nabla\eta_0)^{\mathrm{T}} & -\gamma \end{bmatrix}, \; \mathbf{B}_3 = \begin{bmatrix} 0 & 0 & 0 & 0 & 0 & 0 & 0 & 0 \\ 0 & 0 & 0 & 0 & 0 & 0 & 0 & 0 \\ c_1 & c_1 & c_1 & c_1 & c_1 & c_1 & 2\eta_0 c_3 & c_2 \end{bmatrix} \tag{27}$$

with $c_1 = \frac{\gamma(\gamma-1)M_r^2}{Re}\frac{\eta_0}{2}$, $c_2 = -\frac{2}{3}\eta_0\frac{\gamma(\gamma-1)M_r^2}{Re}$, and $c_3 = \frac{\gamma}{RePr}$. Next, we describe the approximation for the nonlinear terms in the vectors $\mathbf{f}_i$:

$$\mathbf{f}_{1_\chi} = \begin{bmatrix} \xi_\chi \nabla^2 p \\ \xi_\chi \nabla p \\ \xi_\chi (\nabla \cdot \mathbf{u}) \\ \xi_\chi \nabla \cdot \Pi(\mathbf{u}, \eta_0) \\ p_\chi \nabla^2 \xi \\ p_\chi \nabla \xi \\ p_\chi \nabla \cdot \mathbf{u} \end{bmatrix} = \begin{bmatrix} \xi_\chi & 0 & 0 & 0 & 0 & 0 & 0 \\ 0 & \xi_\chi \mathbf{I}_3 & 0 & 0 & 0 & 0 & 0 \\ 0 & 0 & \xi_\chi & 0 & 0 & 0 & 0 \\ 0 & 0 & 0 & \xi_\chi \mathbf{I}_3 & 0 & 0 & 0 \\ 0 & 0 & 0 & 0 & p_\chi & 0 & 0 \\ 0 & 0 & 0 & 0 & 0 & p_\chi \mathbf{I}_3 & 0 \\ 0 & 0 & 0 & 0 & 0 & 0 & p_\chi \end{bmatrix} \begin{bmatrix} \nabla^2 p \\ \nabla p \\ \nabla \cdot \mathbf{u} \\ \nabla \cdot \Pi(\mathbf{u}, \eta_0) \\ \nabla^2 \xi \\ \nabla \xi \\ \nabla \cdot \mathbf{u} \end{bmatrix} = \bar{\Delta}_1 \mathbf{y}_1, \tag{28}$$

$$\mathbf{f}_{2_\chi} = \begin{bmatrix} \mathbf{u}_\chi \cdot \nabla \xi \\ \mathbf{u}_\chi \cdot \nabla u \\ \mathbf{u}_\chi \cdot \nabla v \\ \mathbf{u}_\chi \cdot \nabla w \\ \mathbf{u}_\chi \cdot \nabla p \end{bmatrix} = \begin{bmatrix} \mathbf{u}_\chi^{\mathrm{T}} & 0 & 0 & 0 & 0 \\ 0 & \mathbf{u}_\chi^{\mathrm{T}} & 0 & 0 & 0 \\ 0 & 0 & \mathbf{u}_\chi^{\mathrm{T}} & 0 & 0 \\ 0 & 0 & 0 & \mathbf{u}_\chi^{\mathrm{T}} & 0 \\ 0 & 0 & 0 & 0 & \mathbf{u}_\chi^{\mathrm{T}} \end{bmatrix} \begin{bmatrix} \nabla \xi \\ \nabla u \\ \nabla v \\ \nabla w \\ \nabla p \end{bmatrix} = \bar{\Delta}_2 \mathbf{y}_2, \tag{29}$$

$$\begin{aligned} \mathbf{f}_{3_\chi} &= \begin{bmatrix} (\nabla u)_\chi \cdot \nabla u \\ (\nabla v)_\chi \cdot \nabla v \\ (\nabla w)_\chi \cdot \nabla w \\ (\partial_x \mathbf{u})_\chi \cdot (2\nabla u + \partial_x \mathbf{u}) \\ (\partial_y \mathbf{u})_\chi \cdot (2\nabla v + \partial_y \mathbf{u}) \\ (\partial_z \mathbf{u})_\chi \cdot (2\nabla w + \partial_z \mathbf{u}) \\ (\nabla p)_\chi \cdot \nabla \xi \\ (\nabla \cdot \mathbf{u})_\chi (\nabla \cdot \mathbf{u}) \end{bmatrix} \\ &= \begin{bmatrix} (\nabla u)_\chi^{\mathrm{T}} & 0 & 0 & 0 & 0 & 0 & 0 & 0 \\ 0 & (\nabla v)_\chi^{\mathrm{T}} & 0 & 0 & 0 & 0 & 0 & 0 \\ 0 & 0 & (\nabla w)_\chi^{\mathrm{T}} & 0 & 0 & 0 & 0 & 0 \\ 0 & 0 & 0 & (\partial_x \mathbf{u})_\chi^{\mathrm{T}} & 0 & 0 & 0 & 0 \\ 0 & 0 & 0 & 0 & (\partial_y \mathbf{u})_\chi^{\mathrm{T}} & 0 & 0 & 0 \\ 0 & 0 & 0 & 0 & 0 & (\partial_z \mathbf{u})_\chi^{\mathrm{T}} & 0 & 0 \\ 0 & 0 & 0 & 0 & 0 & 0 & (\nabla p)_\chi^{\mathrm{T}} & 0 \\ 0 & 0 & 0 & 0 & 0 & 0 & 0 & (\nabla \cdot \mathbf{u})_\chi \end{bmatrix} \begin{bmatrix} \nabla u \\ \nabla v \\ \nabla w \\ (2\nabla u + \partial_x \mathbf{u}) \\ (2\nabla v + \partial_y \mathbf{u}) \\ (2\nabla w + \partial_z \mathbf{u}) \\ \nabla \xi \\ (\nabla \cdot \mathbf{u}) \end{bmatrix} \\ &= \bar{\Delta}_3 \mathbf{y}_3. \end{aligned} \tag{30}$$

Therefore, the entire vector $\mathbf{f}$ is approximated as

$$\mathbf{f}_\chi = \begin{bmatrix} \mathbf{f}_{1_\chi} \\ \mathbf{f}_{2_\chi} \\ \mathbf{f}_{3_\chi} \end{bmatrix} = \mathrm{diag}\left(\bar{\Delta}_1, \bar{\Delta}_2, \bar{\Delta}_3\right) \begin{bmatrix} \mathbf{y}_1 \\ \mathbf{y}_2 \\ \mathbf{y}_3 \end{bmatrix} = \mathrm{diag}\left(\Delta_1, \Delta_2, \ldots, \Delta_{11}\right) \mathbf{y} = \Delta \mathbf{y} \tag{31}$$

where

$$\begin{aligned} &\Delta_1 = \xi_\chi \mathbf{I}_8, \quad \Delta_2 = p_\chi \mathbf{I}_5, \quad \Delta_3 = \mathbf{I}_5 \otimes \mathbf{u}_\chi^{\mathrm{T}}, \quad \Delta_4 = (\nabla u)_\chi^{\mathrm{T}}, \quad \Delta_5 = (\nabla v)_\chi^{\mathrm{T}}, \quad \Delta_6 = (\nabla w)_\chi^{\mathrm{T}}, \\ &\Delta_7 = (\partial_x \mathbf{u})_\chi^{\mathrm{T}}, \quad \Delta_8 = (\partial_y \mathbf{u})_\chi^{\mathrm{T}}, \quad \Delta_9 = (\partial_z \mathbf{u})_\chi^{\mathrm{T}}, \quad \Delta_{10} = (\nabla p)_\chi^{\mathrm{T}}, \quad \Delta_{11} = (\nabla \cdot \mathbf{u})_\chi. \end{aligned} \tag{32}$$

The vectors $\mathbf{y}_i$ can be expressed in terms of the perturbed quantities $(\xi, \mathbf{u}, p)$ as follows:

$$\mathbf{y}_1 = \begin{bmatrix} \nabla^2 p \\ \nabla p \\ \nabla \cdot \mathbf{u} \\ \nabla \cdot \Pi(\mathbf{u}, \eta_0) \\ \nabla^2 \xi \\ \nabla \xi \\ \nabla \cdot \mathbf{u} \end{bmatrix} = \mathbf{C}_1 \begin{bmatrix} \xi \\ u \\ v \\ w \\ p \end{bmatrix}, \quad \mathbf{y}_2 = \begin{bmatrix} \nabla \xi \\ \nabla u \\ \nabla v \\ \nabla w \\ \nabla p \end{bmatrix} = \mathbf{C}_2 \begin{bmatrix} \xi \\ u \\ v \\ w \\ p \end{bmatrix}, \tag{33}$$

where

$$\mathbf{C}_1 = \begin{bmatrix} 0 & 0 & 0 & 0 & \nabla^2 \\ 0 & 0 & 0 & 0 & \nabla \\ 0 & \partial_x & \partial_y & \partial_z & 0 \\ 0 & C_{\Pi_{11}} & C_{\Pi_{12}} & C_{\Pi_{13}} & 0 \\ 0 & C_{\Pi_{21}} & C_{\Pi_{22}} & C_{\Pi_{23}} & 0 \\ 0 & C_{\Pi_{31}} & C_{\Pi_{32}} & C_{\Pi_{33}} & 0 \\ \nabla^2 & 0 & 0 & 0 & 0 \\ \nabla & 0 & 0 & 0 & 0 \\ 0 & \partial_x & \partial_y & \partial_z & 0 \end{bmatrix}, \quad \mathbf{C}_2 = \begin{bmatrix} \nabla & 0 & 0 & 0 & 0 \\ 0 & \nabla & 0 & 0 & 0 \\ 0 & 0 & \nabla & 0 & 0 \\ 0 & 0 & 0 & \nabla & 0 \\ 0 & 0 & 0 & 0 & \nabla \end{bmatrix}, \tag{34}$$

with

$$\begin{aligned} &C_{\Pi_{11}} = \eta_0 \nabla^2 + \frac{1}{3}\eta_0 \partial_{xx} + \eta_0' \partial_y, \quad C_{\Pi_{12}} = \frac{1}{3}\eta_0 \partial_{xy} + \eta_0' \partial_x, \quad C_{\Pi_{13}} = \frac{1}{3}\eta_0 \partial_{xz}, \\ &C_{\Pi_{21}} = \frac{1}{3}\eta_0 \partial_{xy} - \frac{2}{3}\eta_0' \partial_x, \quad C_{\Pi_{22}} = \eta_0 \nabla^2 + \frac{1}{3}\eta_0 \partial_{yy} + \frac{4}{3}\eta_0' \partial_y, \quad C_{\Pi_{23}} = \frac{1}{3}\eta_0 \partial_{yz} - \frac{2}{3}\eta_0' \partial_z, \\ &C_{\Pi_{31}} = \frac{1}{3}\eta_0 \partial_{xz}, \quad C_{\Pi_{32}} = \frac{1}{3}\eta_0 \partial_{yz} + \eta_0' \partial_z, \quad C_{\Pi_{33}} = \eta_0 \nabla^2 + \frac{1}{3}\eta_0 \partial_{zz} + \eta_0' \partial_y. \end{aligned} \tag{35}$$

Also, we have

$$\mathbf{y}_3 = \begin{bmatrix} \nabla u \\ \nabla v \\ \nabla w \\ (2\nabla u + \partial_x \mathbf{u}) \\ (2\nabla v + \partial_y \mathbf{u}) \\ (2\nabla w + \partial_z \mathbf{u}) \\ \nabla \xi \\ (\nabla \cdot \mathbf{u}) \end{bmatrix} = \mathbf{C}_{3_1} \begin{bmatrix} \nabla u \\ \nabla v \\ \nabla w \\ \partial_x \mathbf{u} \\ \partial_y \mathbf{u} \\ \partial_z \mathbf{u} \\ \nabla \xi \end{bmatrix} = \mathbf{C}_{3_1} \mathbf{C}_{3_2} \begin{bmatrix} \xi \\ u \\ v \\ w \\ p \end{bmatrix} \tag{36}$$

where

$$\mathbf{C}_{3_1} = \begin{bmatrix} \mathbf{I}_3 & 0 & 0 & 0 & 0 & 0 & 0 \\ 0 & \mathbf{I}_3 & 0 & 0 & 0 & 0 & 0 \\ 0 & 0 & \mathbf{I}_3 & 0 & 0 & 0 & 0 \\ 2\mathbf{I}_3 & 0 & 0 & \mathbf{I}_3 & 0 & 0 & 0 \\ 0 & 2\mathbf{I}_3 & 0 & 0 & \mathbf{I}_3 & 0 & 0 \\ 0 & 0 & 2\mathbf{I}_3 & 0 & 0 & \mathbf{I}_3 & 0 \\ 0 & 0 & 0 & 0 & 0 & 0 & \mathbf{I}_3 \\ \begin{bmatrix} 1 & 0 & 0 \end{bmatrix} & \begin{bmatrix} 0 & 1 & 0 \end{bmatrix} & \begin{bmatrix} 0 & 0 & 1 \end{bmatrix} & 0 & 0 & 0 & 0 \end{bmatrix}, \quad \mathbf{C}_{3_2} = \begin{bmatrix} 0 & \nabla & 0 & 0 & 0 \\ 0 & 0 & \nabla & 0 & 0 \\ 0 & 0 & 0 & \nabla & 0 \\ 0 & \partial_x & 0 & 0 & 0 \\ 0 & 0 & \partial_x & 0 & 0 \\ 0 & 0 & 0 & \partial_x & 0 \\ 0 & \partial_y & 0 & 0 & 0 \\ 0 & 0 & \partial_y & 0 & 0 \\ 0 & 0 & 0 & \partial_y & 0 \\ 0 & \partial_z & 0 & 0 & 0 \\ 0 & 0 & \partial_z & 0 & 0 \\ 0 & 0 & 0 & \partial_z & 0 \\ \nabla & 0 & 0 & 0 & 0 \end{bmatrix}. \tag{37}$$

Hence, we finally have

$$\mathbf{y} = \begin{bmatrix} \mathbf{y}_1 \\ \mathbf{y}_2 \\ \mathbf{y}_3 \end{bmatrix} = \begin{bmatrix} \mathbf{C}_1 \\ \mathbf{C}_2 \\ \mathbf{C}_{3_1}\mathbf{C}_{3_2} \end{bmatrix} \begin{bmatrix} \xi \\ u \\ v \\ w \\ p \end{bmatrix} = \mathbf{C}_y \begin{bmatrix} \xi \\ u \\ v \\ w \\ p \end{bmatrix}. \tag{38}$$

Therefore, the overall perturbation dynamics obtained through the modeling is given by

$$\begin{bmatrix} \partial_t \xi \\ \partial_t \mathbf{u} \\ \partial_t p \end{bmatrix} = \begin{bmatrix} L_\xi(\mathbf{q}) \\ L_\mathbf{u}(\mathbf{q}) \\ L_p(\mathbf{q}) \end{bmatrix} + \mathbf{B}\mathbf{f}_\chi, \quad \mathbf{y} = \mathbf{C}_y \begin{bmatrix} \xi & \mathbf{u}^\mathrm{T} & p \end{bmatrix}^\mathrm{T}, \quad \mathbf{f}_\chi = \Delta\mathbf{y} \tag{39}$$

which is discretized using the Fourier-Chebyshev-Fourier spectral discretization. The discretized equations (with $\hat{(\cdot)}$ denoting the discretized quantities) can be expressed in the following form:

$$\begin{aligned} \mathbf{i}\omega\hat{\mathbf{q}} &= \hat{\mathbf{L}}(k_x, k_z)\hat{\mathbf{q}} + \hat{\mathbf{B}}\hat{\mathbf{f}}_\chi \\ \hat{\mathbf{y}} &= \hat{\mathbf{C}}_y(k_x, k_z)\hat{\mathbf{q}} \\ \hat{\mathbf{f}}_\chi &= \mathrm{diag}\left(\hat{\Delta}_1, \hat{\Delta}_2, \ldots, \hat{\Delta}_{11}\right)\hat{\mathbf{y}} = \hat{\Delta}\hat{\mathbf{y}} \end{aligned} \tag{40}$$

where k_x and k_z are the wavenumbers along the streamwise (x) and spanwise (z) directions, respectively, ω is the temporal frequency, $\hat{\mathbf{L}}(k_x, k_z) \in \mathbb{C}^{n_q \times n_q}$, $\hat{\mathbf{C}}_y(k_x, k_z) \in \mathbb{C}^{n_y \times n_q}$ are the discretized operators (see Appendix A for details on the discretized operators), and $\hat{\mathbf{B}} \in \mathbb{R}^{n_q \times n_f}$ is the dimensionally consistent form of $\mathbf{B}$ for the discretized variables. Thus, we have $n_q = 5N_y$ where N_y denotes the number of Chebyshev collocation points in the wall-normal (y) direction. Also in the above, each $\hat{\Delta}_i$ is a complex block matrix, with $\hat{\Delta}_3$ containing a repeated full-block structure (i.e., a single full block repeated 5 times, see (32)). Note that we do not exploit this repeated full-block structure in the current study, but plan to do so in our future work.

For a given tuple (k_x, k_z, ω), the system of equations in (40) can be interpreted as a feedback interconnection between a linear time invariant (LTI) system and a structured uncertainty $\hat{\Delta}$. In this interpretation, the inputs and outputs of the LTI system are $\hat{\mathbf{f}}_\chi \in \mathbb{C}^{n_f}$ and $\hat{\mathbf{y}} \in \mathbb{C}^{n_y}$, respectively. Furthermore, the I/O relationship can be written as

$$\hat{\mathbf{y}} = \mathcal{H}(k_x, k_z, \omega)\hat{\mathbf{f}}_\chi \tag{41}$$

where $\mathcal{H}(k_x, k_z, \omega) = \hat{\mathbf{C}}_y(k_x, k_z)(\mathbf{i}\omega\mathbf{I}_{n_q} - \hat{\mathbf{L}}(k_x, k_z))^{-1}\hat{\mathbf{B}}$ is the frequency response operator. Figure 3 schematically outlines how the continuous-time modeling of the perturbation dynamics leads to the equivalent discretized system.

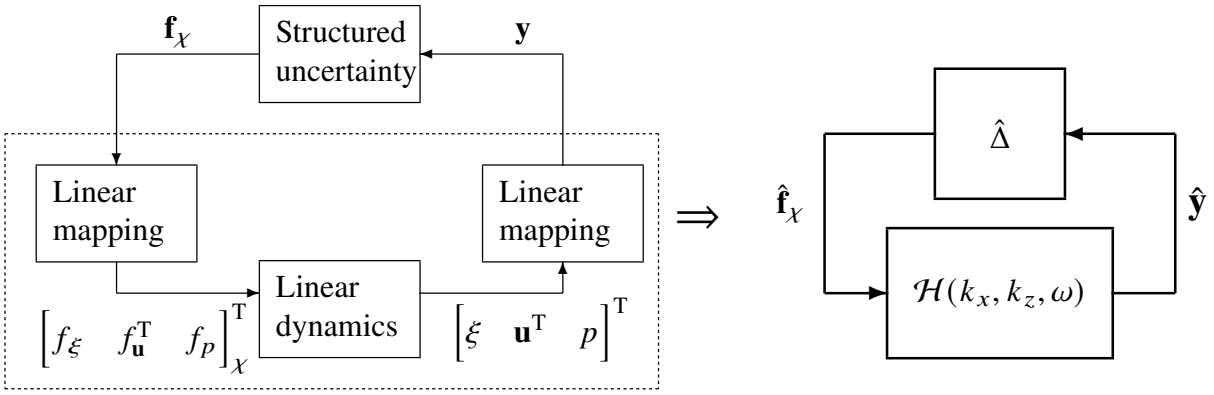

Fig. 3 The models of perturbation dynamics - continuous-time form (left) and discretized form (right).

D. Code validation: Eigenvalue spectra

For the purposes of code validation, we compare eigenvalues of the discretized linear operator $\hat{\mathbf{L}}(k_x, k_z)$ with eigenvalues of the equivalent operator for the standard (cubic) description of compressible NSE. Following the common practice in the literature [8, 23, 24], the eigenvalues (λ) are plotted in terms of the complex wavespeed $c = \lambda/k_x = c_r + \mathbf{i}c_i$. The comparison results are shown in Fig. 4 where we have utilized $k_x = k_z = 0.1$, $Re = 2 \times 10^5$, $M_r = 2$, $Pr = 0.72$, $N_y = 200$. As shown in Fig. 4, both sets of eigenvalues match, and these results are also consistent with results in the literature (see, for example, [8]).

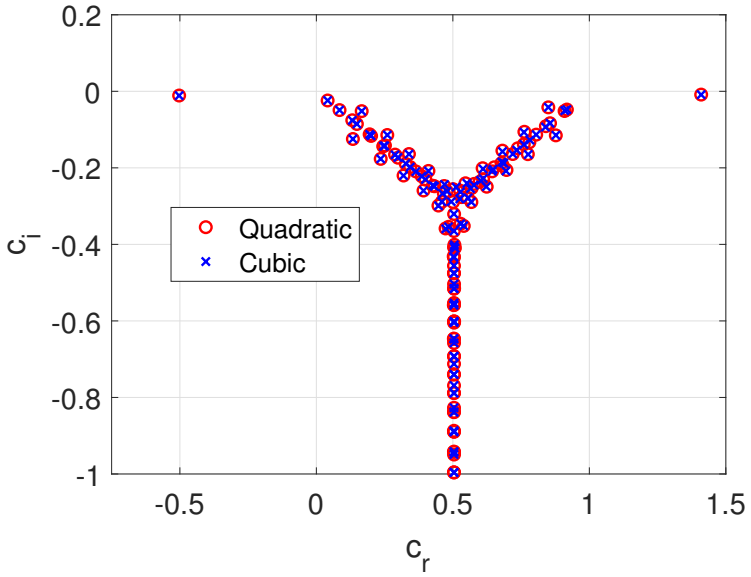

Fig. 4 Eigenvalue spectra of the linear operators for $k_x = k_z = 0.1$, $Re = 2 \times 10^5$, $M_r = 2$, $Pr = 0.72$, $N_y = 200$.

E. Structured I/O Analysis: Structured Singular Value

As stated before, the structured I/O analysis utilizes the concept of structured singular value (SSV or μ). We will start the discussion with the matrix case by recalling the definition of μ for a given matrix $\mathbf{H} \in \mathbb{C}^{n\times m}$ and a set of structured matrices $\mathbf{\Delta} \subset \mathbb{C}^{m\times n}$.

Definition 1 ([18, 26]) *For a given matrix $\mathbf{H} \in \mathbb{C}^{n\times m}$ and a set of structured matrices $\mathbf{\Delta} \subset \mathbb{C}^{m\times n}$, the structured singular value is defined as*

$$\mu_\mathbf{\Delta}(\mathbf{H}) = \frac{1}{\min(\|\hat{\Delta}\|_2 : \hat{\Delta} \in \mathbf{\Delta}, \det(\mathbf{I}_n - \mathbf{H}\hat{\Delta}) = 0)}. \tag{42}$$

If there does not exist $\hat{\Delta} \in \mathbf{\Delta}$ *such that* $\det(\mathbf{I}_n - \mathbf{H}\hat{\Delta}) = 0$*, then* $\mu_{\mathbf{\Delta}}(\mathbf{H}) = 0$*.*

Note that $\mu_{\mathbf{\Delta}}(\mathbf{H})$ depends both on the matrix $\mathbf{H}$ and the set $\mathbf{\Delta}$. Also, SSV is inversely related to the smallest structured uncertainty $\hat{\Delta}$ (in the sense of $\|\cdot\|_2$) that can make the feedback interconnection of the form shown in Fig. 3 (right) unstable (see Remark 3.4 in [18] for more details). Thus, SSV is closely related to flow stability, i.e., a large value indicates that the system is sensitive to small perturbations that can cause instability and vice versa [26]. For the frequency response operator $\mathcal{H}(k_x, k_z, \omega)$ at a given wavenumber pair (k_x, k_z), computing SSV reduces to computing the $\mu_{\mathbf{\Delta}}(\mathcal{H}(k_x, k_z, \omega))$ on a grid of temporal frequencies ω. This approach essentially provides information about wavenumber pairs (k_x, k_z) where the SSV is higher, thereby indicating an instability mechanism. However, exactly computing the SSV is NP-hard for a general uncertainty structure [27–29]. As a result, it is a common practice to compute upper and lower bounds on the SSV instead. Specifically in this paper, we are interested in calculating an upper bound, which provides a sufficient condition for robust stability [18, 19, 30–32]. Details on the upper bound calculation are provided next.

By definition, we have $\mu(\mathbf{H}) \leq \|\mathbf{H}\|_2$ [18]. Furthermore, for each set of uncertainties $\mathbf{\Delta} \subset \mathbb{C}^{m\times n}$, there are sets of non-singular matrices $\mathbb{D}_1 \subset \mathbb{C}^{n\times n}$, $\mathbb{D}_2 \subset \mathbb{C}^{m\times m}$ such that $\hat{\Delta}\mathbf{D}_1 = \mathbf{D}_2\hat{\Delta}$ for any $\mathbf{D}_1 \in \mathbb{D}_1, \mathbf{D}_2 \in \mathbb{D}_2, \hat{\Delta} \in \mathbf{\Delta}$. Therefore, $\det(\mathbf{I}_n - \mathbf{H}\hat{\Delta}) = \det(\mathbf{I}_n - \mathbf{H}\mathbf{D}_2^{-1}\hat{\Delta}\mathbf{D}_1) = \det(\mathbf{I}_m - \hat{\Delta}\mathbf{D}_1\mathbf{H}\mathbf{D}_2^{-1}) = \det(\mathbf{I}_n - \mathbf{D}_1\mathbf{H}\mathbf{D}_2^{-1}\hat{\Delta})$ which means $\mu_{\mathbf{\Delta}}(\mathbf{H}) = \mu_{\mathbf{\Delta}}(\mathbf{D}_1\mathbf{H}\mathbf{D}_2^{-1})$. This can be used to tighten the upper bound as

$$\mu_{\mathbf{\Delta}}(\mathbf{H}) \leq \min_{\mathbf{D}_1\in\mathbb{D}_1,\ \mathbf{D}_2\in\mathbb{D}_2} \|\mathbf{D}_1\mathbf{H}\mathbf{D}_2^{-1}\|_2. \tag{43}$$

The upper bound is called the D-scale upper bound. In this paper, we consider the uncertainty to consist of non-repeating full blocks, i.e., we take $\mathbf{\Delta}_{nr} = \{\mathrm{diag}(\hat{\Delta}_1, \hat{\Delta}_2, \ldots, \hat{\Delta}_{15}) : \hat{\Delta}_i \in \mathbb{C}^{m_i\times n_i}\}$ with $\sum_{i=1}^{15} m_i = n_f$ and $\sum_{i=1}^{15} n_i = n_y$ for consistent dimensions. Note that the 5 repeated full blocks in $\hat{\Delta}_3$ are approximated with non-repeating ones in this setting. Due to this structure of $\mathbf{\Delta}_{nr}$, the corresponding sets of the scaling matrices take the following diagonal form:

$$\begin{aligned}
\mathbb{D}_{1_{nr}} &= \{\mathrm{diag}(d_1\mathbf{I}_{n_1}, d_2\mathbf{I}_{n_2}, \ldots, d_{15}\mathbf{I}_{n_{15}}) : d_i > 0,\ i = 1, 2, \ldots, 15\},\\
\mathbb{D}_{2_{nr}} &= \{\mathrm{diag}(d_1\mathbf{I}_{m_1}, d_2\mathbf{I}_{m_2}, \ldots, d_{15}\mathbf{I}_{m_{15}}) : d_i > 0,\ i = 1, 2, \ldots, 15\}.
\end{aligned} \tag{44}$$

Thus, the optimization problem for the D-scale upper bounds in (43) reduces to solving for the optimal scalars d_i. This can be posed as a generalized eigenvalue problem [18, 19]. However, this approach is computationally expensive for large-dimensional problems. Instead, utilizing a weaker bound $\|\mathbf{D}_1\mathbf{H}\mathbf{D}_2^{-1}\|_2 \leq \|\mathbf{D}_1\mathbf{H}\mathbf{D}_2^{-1}\|_F$ is often sufficient for practical purposes [33]. In this case, an upper bound for a given matrix $\mathbf{H}$ becomes

$$\mu_{\mathbf{\Delta}}(\mathbf{H}) \leq \min_{\mathbf{D}_1\in\mathbb{D}_{1_{nr}},\ \mathbf{D}_2\in\mathbb{D}_{2_{nr}}} \|\mathbf{D}_1\mathbf{H}\mathbf{D}_2^{-1}\|_F. \tag{45}$$

The optimization problem on the right-hand side of (45) can be efficiently solved using a variation of the standard Osborne's iterations [34]. Details on the particular variation used in this paper can be found in [20].

In terms of the frequency response operator $\mathcal{H}(k_x, k_z, \omega)$ at a given wavenumber pair (k_x, k_z) and the uncertainty set $\mathbf{\Delta}_{nr}$, we choose the 'best' upper bound, denoted by $\alpha_\mu(k_x, k_z)$, as the maximum of the upper bounds computed on a temporal frequency (ω) grid. This is given by

$$\alpha_\mu(k_x, k_z) = \max_{\omega\in\Omega}\left[\min_{\mathbf{D}_1\in\mathbb{D}_{1_{nr}},\ \mathbf{D}_2\in\mathbb{D}_{2_{nr}}} \|\mathbf{D}_1\mathcal{H}(k_x, k_z, \omega)\mathbf{D}_2^{-1}\|_F\right] \tag{46}$$

where $\Omega \subset \mathbb{R}$ is the ω grid.

For comparison with the SSV upper bounds, we compute the H_∞ norm and resolvent gain at each wavenumber pair (k_x, k_z), respectively denoted by $\|\mathcal{H}\|_\infty(k_x, k_z)$ and $\sigma_R(k_x, k_z)$, as

$$\begin{aligned}
\|\mathcal{H}\|_\infty(k_x, k_z) &= \max_{\omega\in\Omega} \|\mathcal{H}(k_x, k_z, \omega)\|_2,\\
\sigma_R(k_x, k_z) &= \max_{\omega\in\Omega} \|(\mathbf{i}\omega\mathbf{I}_{n_q} - \hat{\mathbf{L}}(k_x, k_z))^{-1}\|_2.
\end{aligned} \tag{47}$$

It should be noted that both the H_∞ norm and resolvent gain calculations are carried out using the quadratic representation of compressible NSE presented here and not the standard cubic formulation in the literature. Also, the input-output model used for the H_∞ norm is as shown in Fig. 3 (right) with the structured uncertainty $\hat{\Delta}$ replaced by the set $\mathbb{C}^{n_f\times n_y}$.

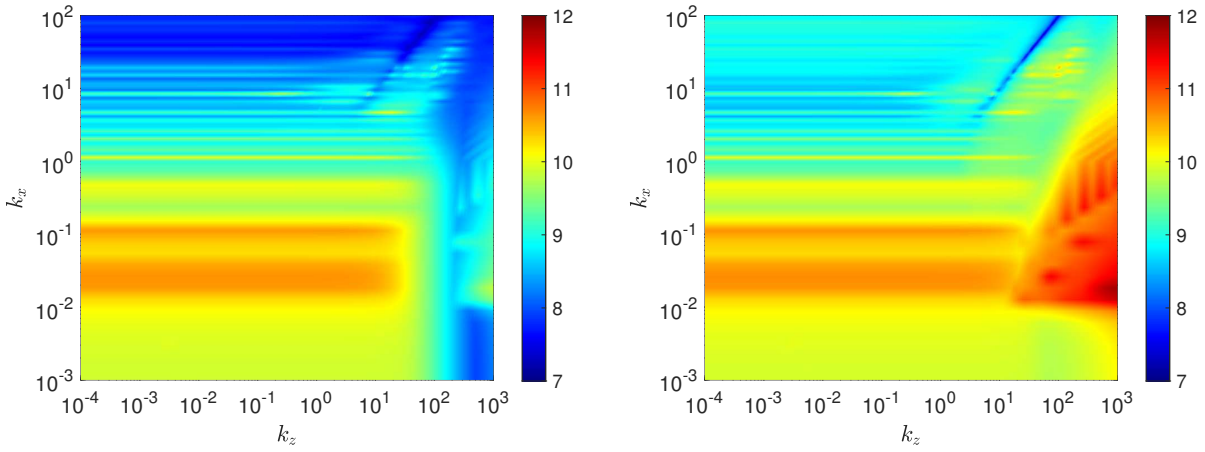

(a) $\log_{10}\left(\alpha_\mu(k_x, k_z)\right)$

(b) $\log_{10}\left(\|\mathcal{H}\|_\infty(k_x, k_z)\right)$

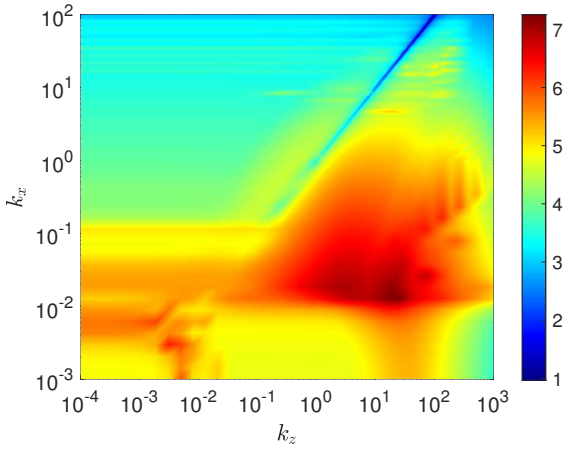

(c) $\log_{10}\left(\sigma_R(k_x, k_z)\right)$

Fig. 5 Distributions of the SSV upper bound, H_∞ norm and resolvent gain over the wavenumer pair (k_x, k_z) grid for $M_r = 0.5$.

IV. Simulation Results

In this section, we will present numerical results for the compressible plane Couette flow by considering a $n_{k_x} \times n_{k_y} \times n_\omega$ grid where n_{k_x}, n_{k_z}, n_ω are the total number of grid points for k_x, k_z, and ω, respectively. We choose $(n_{k_x}, n_{k_z}) = (60, 80)$ logarithmically spaced points for the wavenumbers in the range $k_x \in [10^{-3}, 10^2]$ and $k_z \in [10^{-4}, 10^3]$, and take $n_\omega = 50$ logarithmically spaced points for the temporal frequency in the range $\omega \in [-10, 10]$. Also, we choose other parameter values as $Re = 2 \times 10^5$, $Pr = 0.72$, $N_y = 100$. We will illustrate the results for subsonic ($M_r = 0.5$), transonic ($M_r = 1$), and supersonic ($M_r = 2$) Mach number regimes. All the results in this section are generated using MATLAB R2022a. To provide an estimate of the computation times associated with the SSV upper bounds, we have utilized the 'tic-toc' functionality within MATLAB. These calculations are carried out on a desktop computer with a 12-th Gen Intel(R) Core(TM) i7-12700K processor and 16 GB RAM. Also, computation times for our current implementation of the Osborne's iteration are compared with an inbuilt MATLAB function/command, 'osborne', which implements another variation of the Osborne's iteration. In this setting, the average times required for computing the SSV upper bounds at each (k_x, k_z, ω) tuple on the grid are as shown in Table 1. Our implementation is clearly much faster compared to the inbuilt command and it is mainly achieved by avoiding overheads associated with the inbuilt command.

Table 1 Average computation times for the SSV upper bounds (50 runs)

Implementation	Time (seconds)
Current	2.16
MATLAB's 'osborne' function/command	8.69

The results for a subsonic Mach number ($M_r = 0.5$) are shown in Fig. 5. The consistent feature among all three results is the existence of the horizontal bands of higher values/gains approximately for (a) $k_x \in [10^{-2}, 10^{-1}]$ and $k_z \in [10^{-4}, 10]$ in Figs. 5a, 5b; (b) $k_x \in [10^{-2.5}, 10^{-1.5}]$ and $k_z \in [10^{-4}, 10^{-1}]$ in Fig. 5c. This means that all these methods are predicting some instability mechanisms at the corresponding wavenumber pairs. There is another feature that is common between the SSV upper bound and H_∞ norm results for k_x values approximately higher than 1. These are the narrow ridges followed by narrow valleys as we move up or down the k_x axis (see Figs. 5a, 5b), which seem to indicate other mechanisms of instability. Notably, this feature is not produced in the resolvent gain result and this might be due to the fact that the input-outputs used for resolvent analysis are different than the ones used for the other

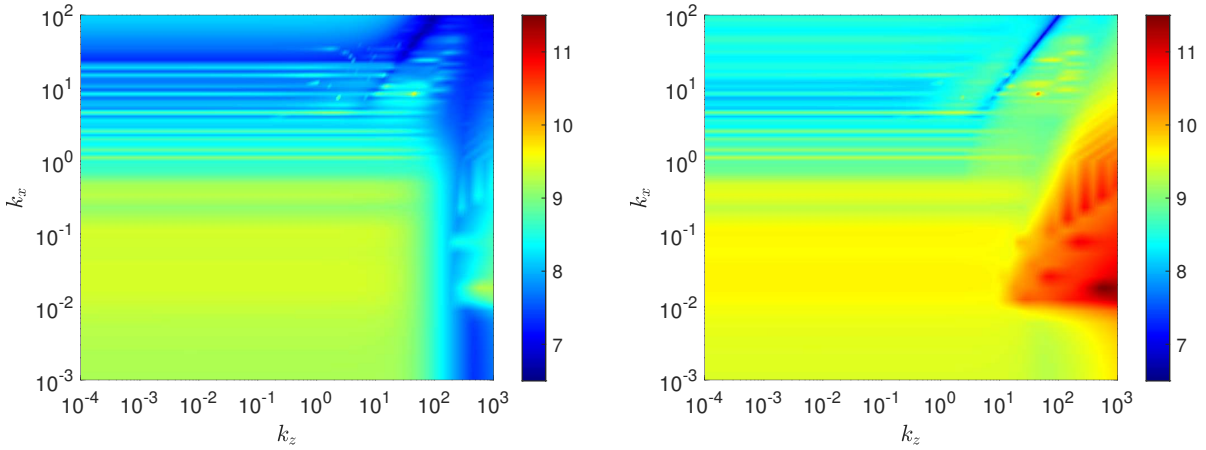

(a) $\log_{10}\left(\alpha_\mu(k_x, k_z)\right)$

(b) $\log_{10}\left(\|\mathcal{H}\|_\infty(k_x, k_z)\right)$

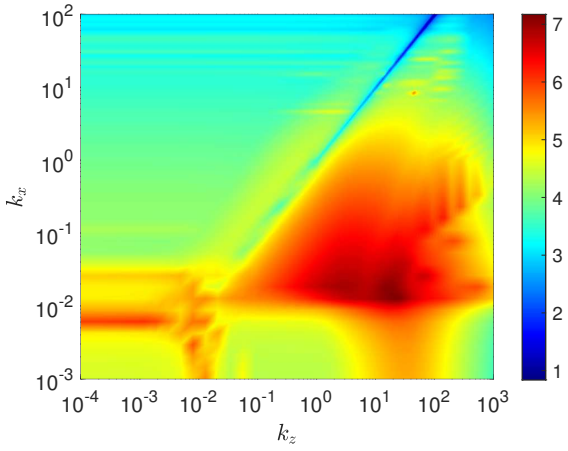

(c) $\log_{10}\left(\sigma_R(k_x, k_z)\right)$

Fig. 6 Distributions of the SSV upper bound, H_∞ norm and resolvent gain over the wavenumer pair (k_x, k_z) grid for $M_r = 1$.

two methods. Note that the H_∞ norm values overall are larger compared to the SSV upper bounds, highlighting the conservatism in the unstructured I/O analysis using the H_∞ norm for this problem. This also means that structured I/O analysis predicts a larger stability margin overall compared to the unstructured I/O analysis. Both the H_∞ norm and resolvent gain results include hotspots with local maxima, although the distribution of these features as a function of the wavenumber pairs is different across the two results (see Figs. 5b, 5c). This particular feature is not present in the SSV upper bound result. Thus, accounting for the structure of the nonlinearity eliminates these instability mechanisms otherwise predicted through the other analysis tools, which might not even represent actual system behavior. Therefore, structured I/O analysis can prove helpful in eliminating potentially redundant instability mechanisms. Furthermore, both the SSV upper bound and H_∞ norm values are much higher compared to the resolvent gain. This is likely due to the outputs utilized in the SSV upper bound and H_∞ analyses containing gradients and higher-order derivatives, whereas the outputs for the resolvent analysis not containing any derivatives (see Sections III.C, III.E).

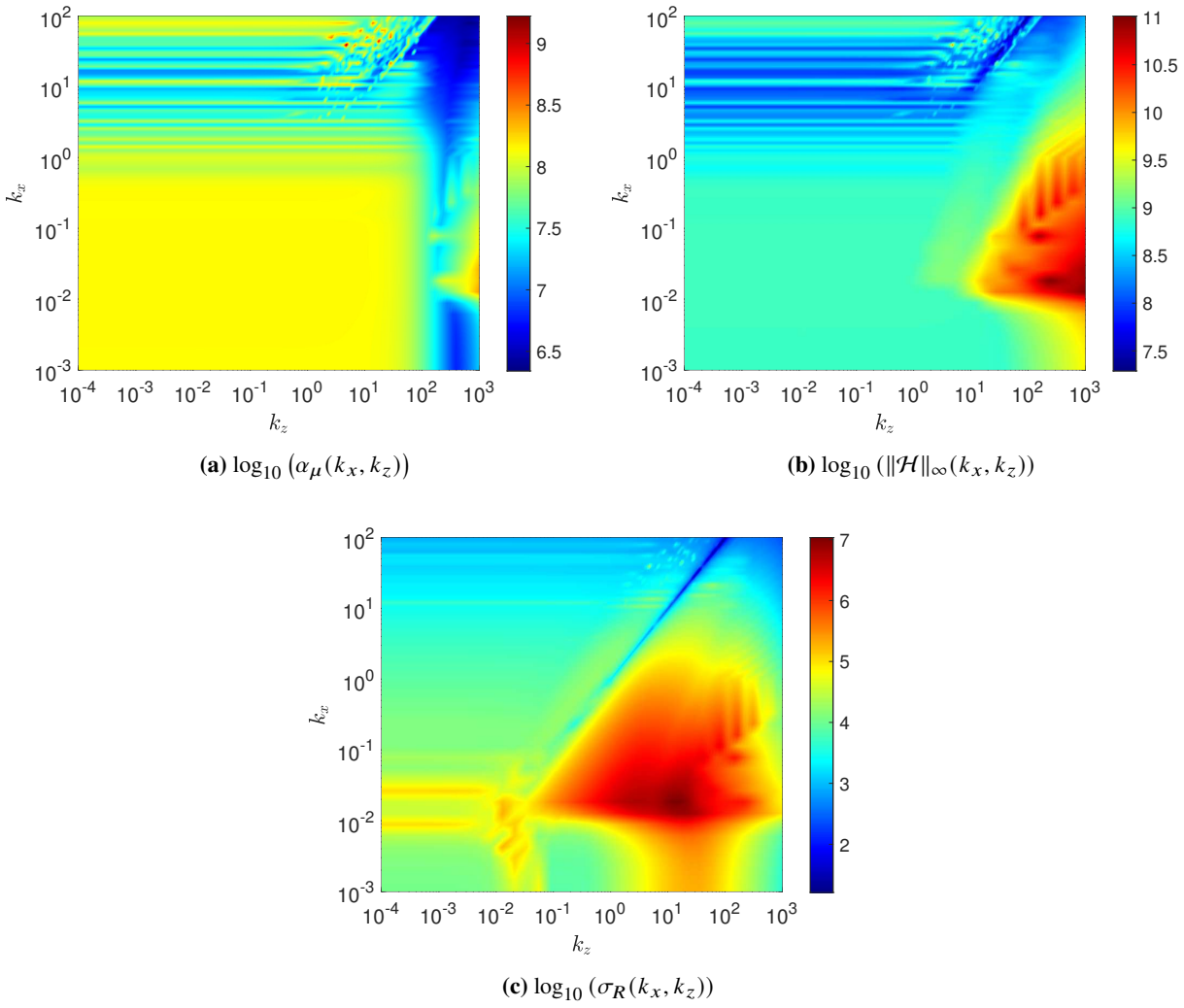

(a) $\log_{10}\left(\alpha_\mu(k_x, k_z)\right)$

(b) $\log_{10}\left(\|\mathcal{H}\|_\infty(k_x, k_z)\right)$

(c) $\log_{10}\left(\sigma_R(k_x, k_z)\right)$

Fig. 7 Distributions of the SSV upper bound, H_∞ norm and resolvent gain over the wavenumer pair (k_x, k_z) grid for $M_r = 2$.

The results for transonic and supersonic Mach numbers are shown in Fig. 6 and Fig. 7, respectively. The overall trends discussed for the subsonic results hold true for these cases as well. On the other hand, the higher-valued horizontal bands in the SSV upper bound and H_∞ norm results, which are present for both the subsonic (see Figs. 5a, 5b) and transonic cases (see Figs. 6a, 6b), disappear in the supersonic results (see Figs. 7a, 7b). Thus, these mechanisms of

instability appear to be a function of the Mach number, with a dominant behavior at lower Mach numbers. Notably, the resolvent gains still continue to predict these mechanisms (albeit in a much diminished manner) for the supersonic case (see Fig. 7c). However, this might be an artifact of the method itself, especially given the consistent predictions by the other two methods here.

V. Conclusion

We have presented a structured input-output analysis tool for compressible flows in this paper. We have derived an exact quadratic representation of the compressible Navier-Stokes equations, which facilitates the subsequent modeling of the nonlinear terms and analysis using the structured singular value formalism. The compressible plane Couette flow is considered as a representative problem. An efficient method for computing the SSV upper bounds is outlined. The numerical results illustrated that the SSV bounds are smaller overall compared to the H_∞ norm results, thereby reducing the conservatism in the unstructured analysis and extending the estimated stability margin of the flow. In addition, SSV analysis identifies qualitatively different instability mechanisms than either H_∞ or resolvent analyses. This indicates that accounting for the structure of the nonlinearity can have profound influence on the eventual interpretation of underlying flow physics. Still, these contradictory observations between the analysis methods considered point towards the need for computational and/or experimental data, which can provide crucial insight into the methods and results discussed in the paper. Our future efforts will involve designing efficient algorithms to exploit the repeated structure of the uncertainty and refine the structured input-output analysis for compressible flows further.

Acknowledgments

This material is based upon work supported by the Air Force Office of Scientific Research under award number FA9550-21-1-0106, the Army Research Office under award number W911NF-20-1-0156, the National Science Foundation under award number CBET-1943988, and the Office of Naval Research under award number N00014-22-1-2029. The authors acknowledge the Minnesota Supercomputing Institute (MSI) at the University of Minnesota for providing the computational resources utilized to generate the numerical results. Maziar S. Hemati is grateful to Scott T.M. Dawson for insightful discussions on compressible resolvent analysis.

References

[1] Taira, K., Hemati, M., and Ukeiley, L., "Modal analysis of fluid flows: Introduction to the virtual collection," *AIAA Journal*, Vol. 58, No. 3, 2020.

[2] Taira, K., Brunton, S. L., Dawson, S. T. M., Rowley, C. W., Tim Colonius, B. J. M., Schmidt, O. T., Gordeyev, S., Theofilis, V., and Ukeiley, L. S., "Modal Analysis of Fluid Flows: An Overview," *AIAA Journal*, Vol. 55, No. 12, 2017.

[3] Taira, K., Hemati, M., Brunton, S., Sun, Y., Duraisamy, K., Bagheri, S., Dawson, S., and Yeh, C.-A., "Modal analysis of fluid flows: Applications and outlook," *AIAA Journal*, Vol. 58, No. 3, 2020.

[4] Jovanović, M. R., "From bypass transition to flow control and data-driven turbulence modeling: an input–output viewpoint," *Annual Review of Fluid Mechanics*, Vol. 35, 2021.

[5] Jovanović, M. R., and Bamieh, B., "Componentwise energy amplification in channel flows," *Journal of Fluid Mechanics*, Vol. 534, 2005, pp. 145–183.

[6] McKeon, B. J., and Sharma, A. S., "A critical-layer framework for turbulent pipe flow," *Journal of Fluid Mechanics*, 2010.

[7] Nichols, J. W., and Candler, G. V., "Input-output analysis of complex hypersonic boundary layers," *AIAA Paper 2019-1383*, 2019.

[8] Dawson, S. T. M., and McKeon, B. J., "Studying the effects of compressibility in planar Couette flow using resolvent analysis," *AIAA Paper 2019-2139*, 2019.

[9] Bae, H. J., Dawson, S. T. M., and McKeon, B. J., "Resolvent-based study of compressibility effects on supersonic turbulent boundary layers," *Journal of Fluid Mechanics*, 2019.

[10] Bae, H. J., Dawson, S. T., and McKeon, B. J., "Studying the effect of wall cooling in supersonic boundary layer flow using resolvent analysis," *AIAA Paper 2020-0575*, 2020.

[11] Sun, Y., Liu, Q., Cattafesta, L. N., and andKunihiko Taira, L. S. U., "Resolvent analysis of compressible laminar and turbulent cavity flows," *AIAA Journal*, Vol. 58, No. 3, 2020.

[12] Kerswell, R., "Nonlinear Nonmodal Stability Theory," *Annual Review of Fluid Mechanics*, Vol. 50, No. 1, 2018, pp. 319–345.

[13] Kalur, A., Seiler, P., and Hemati, M., "Stability and performance analysis of nonlinear and non-normal systems using quadratic constraints," *AIAA Aerospace Sciences Meeting, AIAA Paper 2020-0833*, 2020.

[14] Kalur, A., Seiler, P., and Hemati, M. S., "Nonlinear stability analysis of transitional flows using quadratic constraints," *Physical Review Fluids*, Vol. 6, No. 4, 2021, p. 044401.

[15] Kalur, A., Mushtaq, T., Seiler, P., and Hemati, M. S., "Estimating regions of attraction for transitional flows using quadratic constraints," *IEEE Control Systems Letters*, Vol. 6, 2021, pp. 482–487.

[16] Liu, C., and Gayme, D. F., "Input-output inspired method for permissible perturbation amplitude of transitional wall-bounded shear flows," *Phys. Rev. E*, Vol. 102, 2020, p. 063108.

[17] Liu, C., and Gayme, D. F., "Structured input–output analysis of transitional wall-bounded flows," *Journal of Fluid Mechanics*, Vol. 927, 2021.

[18] Packard, A., and Doyle, J., "The complex structured singular value," *Automatica*, Vol. 29, No. 1, 1993, pp. 71–109.

[19] Zhou, K., Doyle, J., and Glover, K., *Robust and Optimal Control*, Prentice Hall, 1996.

[20] Mushtaq, T., Bhattacharjee, D., Seiler, P., and Hemati, M. S., "Structured Singular Value of a Repeated Complex Full Block Uncertainty," *arXiv preprint arXiv:2211.05929*, 2022.

[21] Mushtaq, T., Bhattacharjee, D., Seiler, P., and Hemati, M. S., "Structured Input-Output Tools for Modal Analysis of a Transitional Channel Flow," *To be presented at the AIAA SciTech Forum 2023*, 2023.

[22] Rowley, C. W., Colonius, T., and Murray, R. M., "Model reduction for compressible flows using POD and Galerkin projection," *Physica D*, Vol. 189, 2004, pp. 115–129.

[23] Duck, P. W., Erlebacher, G., and Hussaini, M. Y., "On the linear stability of compressible plane Couette flow," *Journal of Fluid Mechanics*, Vol. 258, 1994.

[24] Malik, M., Alam, M., and Dey, J., "Nonmodal energy growth and optimal perturbations in compressible plane Couette flow," *Physics of Fluids*, Vol. 18, No. 3, 2006.

[25] Hu, S., and Zhong, Z., "Linear stability of viscous supersonic plane Couette flow," *Physics of Fluids*, Vol. 10, No. 709, 1998.

[26] Zhou, K., and Doyle, J. C., *Essentials of robust control*, Prentice hall Upper Saddle River, NJ, 1998.

[27] Braatz, R. P., Young, P. M., Doyle, J. C., and Morari, M., "Computational complexity of μ calculation," *IEEE Transactions on Automatic Control*, Vol. 39, No. 5, 1994, pp. 1000–1002.

[28] Poljak, S., and Rohn, J., "Checking robust nonsingularity is NP-hard," *Mathematics of Control, Signals and Systems*, Vol. 6, No. 1, 1993, pp. 1–9.

[29] Coxson, G. E., and DeMarco, C. L., "The computational complexity of approximating the minimal perturbation scaling to achieve instability in an interval matrix," *Mathematics of Control, Signals and Systems*, Vol. 7, No. 4, 1994, pp. 279–291.

[30] Dullerud, G. E., and Paganini, F., *A course in robust control theory: a convex approach*, Vol. 36, Springer Science & Business Media, 2013.

[31] Young, P., and Doyle, J., "Computation of mu with real and complex uncertainties," *29th IEEE Conference on Decision and Control*, 1990, pp. 1230–1235 vol.3.

[32] Young, P. M., Newlin, M. P., and Doyle, J. C., "Practical computation of the mixed μ problem," *1992 American Control Conference*, 1992, pp. 2190–2194.

[33] Beck, C., and Doyle, J., "Mixed mu upper bound computation," *Proceedings of the 31st IEEE Conference on Decision and Control*, IEEE, 1992, pp. 3187–3192.

[34] Osborne, E., "On pre-conditioning of matrices," *Journal of the ACM (JACM)*, Vol. 7, No. 4, 1960, pp. 338–345.

A. Discretization of Linear Operators for Perturbation about Base Flow

The discretization is carried out using Chebyshev polynomials in the wall-normal direction and Fourier modes in the streamwise and spanwise directions. The sub-operators of $\hat{\mathbf{L}}$ are given by

$$
\begin{aligned}
L_{\xi,\xi} &= -\mathbf{i}k_x U_0 \\
L_{\xi,u} &= \mathbf{i}k_x \xi_0 \\
L_{\xi,v} &= -\xi_0' + \xi_0 D_y \\
L_{\xi,w} &= \mathbf{i}k_z \xi_0 \\
L_{\xi,p} &= 0 \\
L_{u,\xi} &= 0 \\
L_{u,u} &= -\mathbf{i}k_x U_0 - \frac{\xi_0}{Re}\left[\eta_0\left(\frac{4}{3}k_x^2 - D_{yy} + k_z^2\right) - \eta_0' D_y\right] \\
L_{u,v} &= -U_0' + \mathbf{i}k_x \frac{\xi_0}{3Re}\left[\eta_0 D_y + 3\eta_0'\right] \\
L_{u,w} &= -k_x k_z \frac{\xi_0 \eta_0}{3Re} \\
L_{u,p} &= -\mathbf{i}k_x \frac{\xi_0}{\gamma M_r^2} \\
L_{v,\xi} &= 0 \\
L_{v,u} &= \mathbf{i}k_x \frac{\xi_0}{3Re}\left[\eta_0 D_y - 2\eta_0'\right] \\
L_{v,v} &= -\mathbf{i}k_x U_0 - \frac{\xi_0}{Re}\left[\eta_0\left(k_x^2 - \frac{4}{3}D_{yy} + k_z^2\right) - \frac{4}{3}\eta_0' D_y\right] \\
L_{v,w} &= \mathbf{i}k_z \frac{\xi_0}{3Re}\left[\eta_0 D_y - 2\eta_0'\right] \\
L_{v,p} &= -\frac{\xi_0}{\gamma M_r^2} D_y \\
L_{w,\xi} &= 0 \\
L_{w,u} &= -k_x k_z \frac{\xi_0 \eta_0}{3Re} \\
L_{w,v} &= \mathbf{i}k_z \frac{\xi_0}{3Re}\left[\eta_0 D_y + 3\eta_0'\right] \\
L_{w,w} &= -\mathbf{i}k_x U_0 - \frac{\xi_0}{Re}\left[\eta_0\left(k_x^2 - D_{yy} + \frac{4}{3}k_z^2\right) - \eta_0' D_y\right] \\
L_{w,p} &= -\mathbf{i}k_z \frac{\xi_0}{\gamma M_r^2} \\
L_{p,\xi} &= -\left(\frac{\gamma}{RePr}\right)\left[\eta_0\left(k_x^2 - D_{yy} + k_z^2\right) - \eta_0' D_y\right] \\
L_{p,u} &= -\mathbf{i}k_x \gamma + \frac{\gamma(\gamma-1)M_r^2}{Re}\left(2U_0'\eta_0\right) D_y \\
L_{p,v} &= -\gamma D_y + \mathbf{i}k_x \frac{\gamma(\gamma-1)M_r^2}{Re}\left(2U_0'\eta_0\right) \\
L_{p,w} &= -\mathbf{i}k_z \gamma \\
L_{p,p} &= -\mathbf{i}k_x U_0 + \frac{\gamma}{RePr}\left\{\eta_0\left[\xi_0'' + 2\xi_0' D_y - \xi_0\left(k_x^2 - D_{yy} + k_z^2\right)\right] + \eta_0'(\xi_0' + \xi_0 D_y)\right\}
\end{aligned}
$$

The operators related to $\hat{\mathbf{C}}_y$ are given by

$$\hat{\mathbf{C}}_1 = \begin{bmatrix} 0 & 0 & 0 & 0 & -k_x^2 + D_{yy} - k_z^2 \\ 0 & 0 & 0 & 0 & \mathbf{i}k_x \\ 0 & 0 & 0 & 0 & D_y \\ 0 & 0 & 0 & 0 & \mathbf{i}k_z \\ 0 & \mathbf{i}k_x & D_y & \mathbf{i}k_z & 0 \\ 0 & \hat{C}_{\Pi_{11}} & \hat{C}_{\Pi_{12}} & \hat{C}_{\Pi_{13}} & 0 \\ 0 & \hat{C}_{\Pi_{21}} & \hat{C}_{\Pi_{22}} & \hat{C}_{\Pi_{23}} & 0 \\ 0 & \hat{C}_{\Pi_{31}} & \hat{C}_{\Pi_{32}} & \hat{C}_{\Pi_{33}} & 0 \\ -k_x^2 + D_{yy} - k_z^2 & 0 & 0 & 0 & 0 \\ \mathbf{i}k_x & 0 & 0 & 0 & 0 \\ D_y & 0 & 0 & 0 & 0 \\ \mathbf{i}k_z & 0 & 0 & 0 & 0 \\ 0 & \mathbf{i}k_x & D_y & \mathbf{i}k_z & 0 \end{bmatrix},$$

$$\hat{\mathbf{C}}_2 = \begin{bmatrix} \mathbf{i}k_x & 0 & 0 & 0 & 0 \\ D_y & 0 & 0 & 0 & 0 \\ \mathbf{i}k_z & 0 & 0 & 0 & 0 \\ 0 & \mathbf{i}k_x & 0 & 0 & 0 \\ 0 & D_y & 0 & 0 & 0 \\ 0 & \mathbf{i}k_z & 0 & 0 & 0 \\ 0 & 0 & \mathbf{i}k_x & 0 & 0 \\ 0 & 0 & D_y & 0 & 0 \\ 0 & 0 & \mathbf{i}k_z & 0 & 0 \\ 0 & 0 & 0 & \mathbf{i}k_x & 0 \\ 0 & 0 & 0 & D_y & 0 \\ 0 & 0 & 0 & \mathbf{i}k_z & 0 \\ 0 & 0 & 0 & 0 & \mathbf{i}k_x \\ 0 & 0 & 0 & 0 & D_y \\ 0 & 0 & 0 & 0 & \mathbf{i}k_z \end{bmatrix}, \quad \hat{\mathbf{C}}_{3_2} = \begin{bmatrix} 0 & \mathbf{i}k_x & 0 & 0 & 0 \\ 0 & D_y & 0 & 0 & 0 \\ 0 & \mathbf{i}k_z & 0 & 0 & 0 \\ 0 & 0 & \mathbf{i}k_x & 0 & 0 \\ 0 & 0 & D_y & 0 & 0 \\ 0 & 0 & \mathbf{i}k_z & 0 & 0 \\ 0 & 0 & 0 & \mathbf{i}k_x & 0 \\ 0 & 0 & 0 & D_y & 0 \\ 0 & 0 & 0 & \mathbf{i}k_z & 0 \\ 0 & \mathbf{i}k_x & 0 & 0 & 0 \\ 0 & 0 & \mathbf{i}k_x & 0 & 0 \\ 0 & 0 & 0 & \mathbf{i}k_x & 0 \\ 0 & D_y & 0 & 0 & 0 \\ 0 & 0 & D_y & 0 & 0 \\ 0 & 0 & 0 & D_y & 0 \\ 0 & \mathbf{i}k_z & 0 & 0 & 0 \\ 0 & 0 & \mathbf{i}k_z & 0 & 0 \\ 0 & 0 & 0 & \mathbf{i}k_z & 0 \\ \mathbf{i}k_x & 0 & 0 & 0 & 0 \\ D_y & 0 & 0 & 0 & 0 \\ \mathbf{i}k_z & 0 & 0 & 0 & 0 \end{bmatrix},$$

where

$$\hat{C}_{\Pi_{11}} = \eta_0 \left(-\frac{4}{3}k_x^2 + D_{yy} - k_z^2 \right) + \eta_0' D_y,\ \hat{C}_{\Pi_{12}} = \mathbf{i}k_x \left(\frac{1}{3}\eta_0 D_y + \eta_0' \right),\ \hat{C}_{\Pi_{13}} = -k_x k_z \frac{1}{3}\eta_0,$$

$$\hat{C}_{\Pi_{21}} = \mathbf{i}k_x \left(\frac{1}{3}\eta_0 D_y - \frac{2}{3}\eta_0' \right),\ \hat{C}_{\Pi_{22}} = \eta_0 \left(-k_x^2 + \frac{4}{3}D_{yy} - k_z^2 \right) + \frac{4}{3}\eta_0' D_y,\ \hat{C}_{\Pi_{23}} = \mathbf{i}k_z \left(\frac{1}{3}\eta_0 D_y - \frac{2}{3}\eta_0' \right),$$

$$\hat{C}_{\Pi_{31}} = -k_x k_z \frac{1}{3}\eta_0,\ \hat{C}_{\Pi_{32}} = \mathbf{i}k_z \left(\frac{1}{3}\eta_0 D_y + \eta_0' \right),\ \hat{C}_{\Pi_{33}} = \eta_0 \left(-k_x^2 + D_{yy} - \frac{4}{3}k_z^2 \right) + \eta_0' D_y.$$